

Models of the Compact Jet in GRS 1915+105

Brian Punsly

4014 Emerald Street No.116, Torrance CA, USA 90503
 ICRANet, Piazza della Repubblica 10 Pescara 65100, Italy,
 E-mail: brian.punsly@verizon.net or brian.punsly@comdev-usa.com

15 November 2018

ABSTRACT

In this article, models are constructed of the compact jet in GRS 1915+105 during an epoch of optimal data capture. On April 02, 2003, the object was observed in the hard X-ray/soft gamma ray band (INTEGRAL), hard X-ray band (RXTE), near IR (ESO/New Technology Telescope) and the VLBA (8.3 GHz and 15 GHz). The source was in a so-called "high plateau state." The large radio flux provides high signal to noise ratios in the radio images. Thus, one can image the jet out to large distances ($> 10^{15}$ cm). This combined with the broadband coverage make this epoch the best suited for modeling the jet. The parametric method developed in the papers Ghisellini et al (1985); Ghisellini and Maraschi (1989); Ghisellini et al (1996); Sambruna et al (1997) that has been successfully utilized in the realm of extragalactic radio jets is implemented. The basic model is one where external inverse Compton (EIC) scattering of accretion disk photons by jet plasma provides the hard X-ray powerlaw. Unlike AGN jets, it is found that the radio jet must be highly stratified in the transverse direction in order to produce the observed surface brightness distribution in the radio images. Various jet models are considered. The jet power is $Q \approx 3 - 4 \times 10^{38}$ ergs/sec if the hard X-ray powerlaw luminosity is from EIC in the jet and $Q \approx 2 - 9 \times 10^{37}$ ergs/sec if the X-rays are emitted from the accretion disk corona. These estimates indicate that the jet power can be as high as 60% of the total X-ray luminosity.

Key words: Black hole physics — X-rays: binaries — accretion, accretion disks

Galactic black hole accretion systems might serve as laboratories for AGN (active galactic nuclei) on highly contracted time scales. The black hole candidate, GRS 1915+105, routinely ejects powerful radio emitting plasma out to large distances from the central black hole at relativistic speeds and might be the Galactic analog of radio loud AGN (Rodriguez and Mirabel 1999; Fender et al 1999; Rushton et al 2010a). These major flares are relatively rare compared to the so-called compact jet state (Rushton et al 2010a). A compact, optically thick, elongated structure is frequently observed with long baseline interferometry (Dhawan et al 2000; Fuchs et al 2003; Ribo et al 2004). The low frequency emission is significantly less than in a major flare. It is not clear if there is an analogous structure in the context of AGN. The total power of the jet is also unclear. In this article, the analogy with AGN is pursued by modeling the jet using the standard AGN technique of Ghisellini et al (1985); Ghisellini and Maraschi (1989) with the addition of external Compton scattering (EIC) from (Ghisellini et al 1996; Sambruna et al 1997). There is a correlation or more precisely a direct association of the for-

mation of a compact jet with an excess of hard X-ray emission in the form of a power law (Rushton et al 2010b; Rodriguez et al 2008). The primary assumption of the models of the jet presented below is that this X-ray emission is produced in the base of the jet (Markoff et al 2005). A scenario in which the X-rays are from Compton scattering in the accretion disk corona is also explored briefly in this article with the same techniques.

Since most of the luminosity is in the X-ray band, complete high energy coverage is mandatory for jet modeling. Furthermore, one needs the near IR photometry in multiple bands in order to constrain the synchrotron spectrum. Also, to break the degeneracy in the available models, one requires a faithful representation of the surface brightness distribution of the jet. It is a much simpler task to fit the jet spectrum if the distribution of emissivity is ignored. To meet this challenge in the presence of intrinsic source variability, one needs simultaneous full coverage of the X-ray emission to high frequencies, IR photometry and sensitive VLBA imaging. The only simultaneous set of observations capable of fulfilling these requirements was the campaign

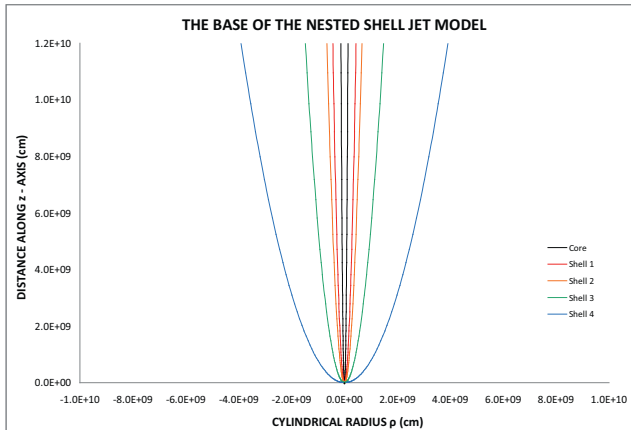


Figure 1. The shell model of transverse jet structure.

presented in (Fuchs et al 2003, 2004). The strongest compact jet ever imaged with VLBA was measured simultaneously in the near IR (ESO/New Technology Telescope) and throughout the hard X-ray and soft gamma ray band (INTEGRAL and RXTE). For more details on the observations see Fuchs et al (2003, 2004).

1 SOME PRELIMINARIES ON JET SPEED

There is uncertainty in the bulk velocity of the compact jet. The Doppler enhancement of the intrinsic radiation is a critical parameter in the determination of the jet power, Q . The Doppler factor, δ , is given in terms of Γ , the Lorentz factor of the outflow; β , the three velocity of the outflow and the angle of propagation to the line of sight, θ ; $\delta = 1/[\Gamma(1 - \beta \cos \theta)]$ (Lind and Blandford 1985). For a jet, the apparent flux density, S_ν is related to the intrinsic value by $S_{\nu, \text{obs}} = \delta^{2+\alpha} S_{\nu, \text{int}}$, where α is the spectral index (the convention adopted in this paper is $S_{\nu} \propto \nu^{-\alpha}$). Assuming an intrinsically symmetric bipolar jet, the elevated flux of the approaching jet has been used to estimate δ . Using a value of $66^\circ < \theta < 70^\circ$ that was deduced from discrete relativistic ejecta at other epochs (see Mirabel and Rodriguez (1994); Fender et al (1999)), estimates of $0.1 < \beta < 0.54$ for the compact jet at various frequencies and epochs of VLBI observations have been obtained (Dhawan et al 2000; Ribo et al 2004). For the epoch April 02, 2003, Ribo et al (2004) found disagreement between the jet velocity inferred from the flux asymmetries of the 15 GHz and 8.3 GHz VLBA images. They reconciled this by looking at the Clean Components, concluding that a value of $\beta = 0.38 \pm 0.04$ was compatible with the data. Thus, $\beta = 0.4$ is the baseline value in the following calculations.

The discussion above is based on direct application of the data to relativistic beaming as was done for discrete ejecta in major flares (Mirabel and Rodriguez 1994; Fender et al 1999). In Dhawan et al (2000), the difference in the directly inferred speeds of the compact jet and the major flares was disconcerting. Thus, they conjectured on other explanations including undetected relativistic motion. Thus, before the Ribo et al (2004) estimated value was adopted in the jet models, an open mind was kept in regards to the value of β . Preliminarily, a relativistic jet was

considered as suggested in Dhawan et al (2000). Assuming $\beta = 0.98$ and $\theta = 66^\circ$ as was deduced from the kinematics of the discrete ejecta in Fender et al (1999), it is found that the flux of blackbody radiation from the accretion disk is highly redshifted in the frame of reference of the jet plasma, so synchrotron self Compton emission (SSC) dominates the external Compton emission (EIC) and SSC is the source of the power law X-rays. Many models were constructed, but because the X-ray luminosity (of the unresolved base of the bipolar jet) observed at earth is redshifted by a factor of δ^4 , the intrinsic X-ray luminosity $L_{\text{int}}(\text{X-ray}) \approx 3.5 \times 10^{40} \text{ erg/sec}$ (Lightman et al 1975). Therefore the jet power, $Q > 3.5 \times 10^{40} \text{ erg/sec}$. This seems unreasonably large. Consequently, relativistic bulk motion is not considered in the following. These calculations indicate that a reasonable model should have at most mildly relativistic velocities that are consistent with the observed jet asymmetry (i.e., $\beta \approx 0.4$). EIC is therefore the source of the power law X-ray hard tail (not SSC) since the redshifted thermal X-ray flux is much larger than the local synchrotron flux within the base of the jet. This result is considered in the context of other estimates of the jet velocity in the literature in the Discussion section.

2 DESCRIPTION OF THE JET MODEL AND THE FIT TO THE DATA

In this section, the parameters in the jet model are defined. One should review Ghisellini et al (1985); Ghisellini and Maraschi (1989) for further discussion. The jet is parameterized in cylindrical coordinates, (ρ, ϕ, z) . The jets models are axisymmetric and have no transverse gradients (this assumption is modified below). The jet shape and axial gradients are parameterized by, z_0 , z_{max} , a , ϵ , m , n , Γ , γ_{min} and γ_{max} through the the expressions,

$$\begin{aligned} \rho &= az^\epsilon; z_0 < z < z_{\text{max}}, N(\gamma) = K\gamma^{-p}, \\ K &= K_0(z/z_0)^{m\epsilon}, B = B_0(z/z_0)^{n\epsilon}. \end{aligned} \quad (1)$$

In equation (1), the electron energy is $E = \gamma m_e c^2$ and the particle number density is $N = \int N(\gamma) d\gamma$. The magnetic field strength is B . The jet begins and ends at z_0 and z_{max} , respectively. The models typically have two regions. The base of the jet is called the paraboloid, which is the stronger inverse Compton source, and it is characterized in Ghisellini et al (1985) by $\epsilon = 0.5$. The outer part of the jet is called the conical region typically with $\epsilon = 1$. This is generalized to other values of ϵ for the outer jet in the following. The outer jet is the primary source of the radio emission. Tables 1 and 2 list the jet model parameters and physical quantities, respectively, that characterize a jet solution. The dimensional input parameters and power law indices in Table 1 define the model in terms of equation 1. The chosen value is either fitted to the data or set by the dimensions of the physical system as noted in the table. All the quantities in Table 2 are physical characteristics of the jet model. It is noted in the table that the values are either an input parameter fitted to the data or a derived physical quantity that is computed from the model. The jet plasma is protonic. Notice that Tables 1 and 2 list four shells and a core (shell 0) instead of one jet. The reason for this necessity was the surface brightness distribution in the VLBA images is very

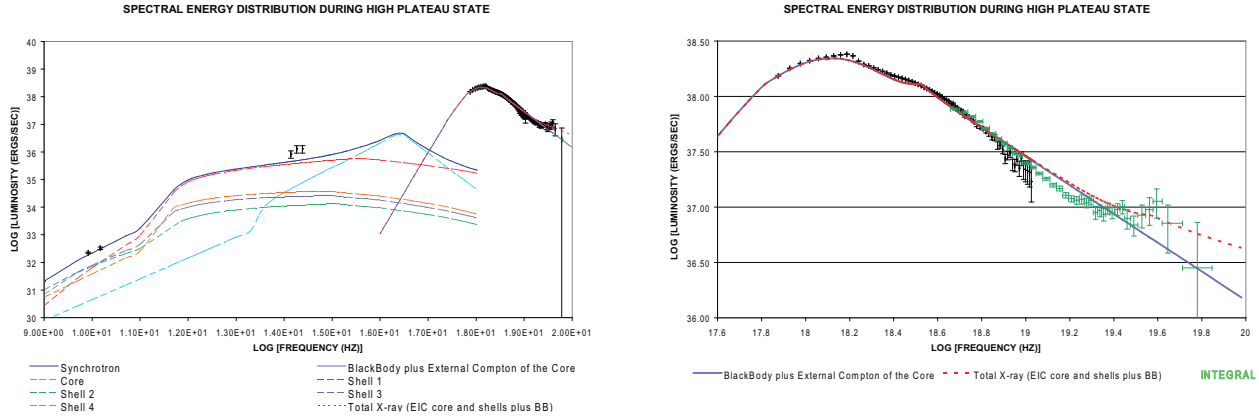


Figure 2. The model fit to the broadband SED is in the left frame. The IR error bars represent the variability at the time of observation from Fuchs et al (2003). The radio data is from a simultaneous VLA measurement at 8.3 GHz and a 15 GHz Ryle telescope observation 2.5 hours earlier. The error bars represent the variability seen in the radio measurements over a two hour time scale (the length of the VLBA observation). This plot includes contributions from the oppositely directed, but otherwise identical counter-jet. The model has an excess above a simple power law in the sub-mm as in the epochs observed in Ogle et al (2000). The right frame is a close-up of the spectral energy distribution in the X-ray region. The INTEGRAL data is in green and the RXTE data is in black. The blue curve is the disk blackbody spectrum plus the EIC steep powerlaw from the core. The red curve also includes the EIC from shells 1 to 4

extended. A jet with no transverse gradients that accurately models the SED always produces a surface brightness distribution that decays too rapidly with z to represent the VLBA maps (see Section 4). Figure 1 shows the relative scale of the nested shells near the base. A continuous transverse gradient would provide a smoother solution. However, the simple crude model of 5 uniform (there are no transverse gradients within each zone) zones is shown to be a reasonably accurate representation of the spectrum and the brightness profile in the following.

Each shell is parameterized in the tables. Columns 2, 3, 4, 10 and 11 of Table 1 define the parameters for the base of the jet in terms of equation (1) for each shell. Similarly, columns 5 - 9 are the outer jet parameters. The initial data surface from which the jet solution begins is formally defined for each shell "i" as the set of points $\rho_{\text{base}}(i-1) < \rho < \rho_{\text{base}}(i)$ such that $z = z_0(\text{base})$, where $z_0(\text{base})$ is the minimum axial coordinate in shell "i" and $\rho_{\text{base}}(i-1) = 0$ for $i = 0$. One important modification to the procedure of Ghisellini et al (1985) is that the inner shells must transfer radiation not only through the optical depth provided by its own synchrotron self absorption, but also that of the surrounding shells. This affects the turnover frequency between the optically thick region of the spectrum and the optically thin region of the spectrum through equation (11) of Ghisellini et al (1985). Because the opacity dies off with cylindrical radius, this is a second order correction to the spectrum from each shell, but is retained to improve the accuracy of the calculations. In the following models, $\theta = 70^\circ$ is assumed as was determined to be consistent with the kinematics of discrete relativistic ejections in Mirabel and Rodriguez (1994). The flux densities are converted to luminosity using a distance of 12.5 kpc to the source as estimated in Mirabel and Rodriguez (1994).

The baseline fit to the broadband spectral energy distribution (SED) is in Figure 2 with the X-ray portion magnified in the right hand frame. These plots are the analog of Figure 5 from Fuchs et al (2003). The X-ray data were calibrated

and reduced with current software suite, HEASOFT V 6.10 and OSA V 9.0, that are improvements from Fuchs et al (2003, 2004). The new results were generously provided by Jerome Rodriguez. The fit in the X-ray region is not that good around 10^{19} Hz. There is increased curvature between 6×10^{18} Hz and 10^{19} Hz that is more evident in the new reduction of the data than in Fuchs et al (2003). There is an overlap of the data in the HEXTE and the INTEGRAL spectrum in this region as discussed in Fuchs et al (2003). Even though the two data sets do not agree in this area (the INTEGRAL spectrum is flatter with higher flux levels, see the related discussion in Fuchs et al (2003)), this does not appear to be the origin of the spectral curvature, but coincidental. This region is not well represented by the EIC powerlaw from the jet core (shell 0) in blue and is actually exacerbated by the spectral hardening that seems to be real at frequencies above 10^{19} Hz. In the model, the hard excess is fit by the red, total luminosity curve which includes a second EIC contribution from the surrounding shells. In this decomposition, the spectral curvature at frequencies just below 10^{19} Hz is consistent with spectral ageing from Compton losses of the higher energy electrons in the core jet which have the shortest radiative time scale, $\tau \sim \gamma^{-2}$ (Tucker 1975). This suggests that a more elaborate jet model is indicated for the core. In Rodriguez et al (2004, 2008), the poor powerlaw fit near 10^{19} Hz is improved by including an inverse Compton coronal component with a thermal cutoff. The extra parameters introduced by a corona with cutoff is beyond the scope of this paper, which is an exploration of how well a simple jet model can explain the data.

Figure 3 is the surface brightness distribution based on the modeled jet emissivity as it would appear with the resolution provided by the synthetic beamwidth of the VLBA as modified by the wavelength dependent interstellar scattering ($\Delta\theta \approx 0.15(\lambda/1\text{cm})^2$ mas) that was determined in Dhawan et al (2000). The plasma in the outer shells produce the low frequency emission from innermost part of the jet, "the radio core" (or peak flux per beamwidth) and the

observed base of the radio jet (the partially resolved emission located within one beamwidth of the core, 33.6 AU at 8.3 GHz and 17.0 AU at 15 GHz) that is depicted by the brightness distribution in Figure 3. Shell 1 produces the farthest reaches of the jet. The lowest contour is at 15 times the RMS noise of the radio images, thus the vertical error bars are very small on all the data points. The dominant source of error is the sparse u-v coverage (the missing 8.3 GHz flux compared to the VLA measurement noted in the figure caption). There is really no way to attach these errors to any of the individual contours. All that one can say is that the relatively long baselines of the VLBA favors missed flux on the least compact scales, the outer-most contours.

3 PHYSICAL INTERPRETATION OF THE JET MODEL

The model presented above and described by the input parameters in Table 1 and Table 2 can be interpreted physically in terms of quantities like mass flux, Poynting flux and magnetic dominance. In the following, it is described how the model parameters relate to physical quantities in Table 2. Column 2 of Table 2 gives the energy flux in each shell at the base. The next 4 columns provide the number density, magnetic field morphology and component strength. Columns 7 and 8 are the ratio of magnetic energy flux to mechanical energy flux at the minimum value of z for each jet region determined from equation (1) and equations (2) - (5), below. The ninth column is the poloidal magnetic flux in the shell determined from the same equations. The last three columns define the electron energy power law from equation (1) that applies throughout the shell.

The innermost shell labeled "0" (the core) is initiated in the innermost part of the accretion disk. In the model, it resides in the ergospheric portion of the disk inside of $1.7 M$ ($M = 2 \times 10^6$ cm in geometrized units for the $14 M_\odot$ black hole mass inferred by Greiner et al (2001)). Thus, one requires a rapidly spinning black hole and a black hole spin of $a/M \geq 0.99$ is necessary to provide sufficient surface area in the disk. If a slowly spinning black hole is used in the model, the volume of the base of the jet increases dramatically and so does Q (which is highly dependent on the total amount of energized particles and magnetic field - large jet volumes create large total plasma energy in the models). The magnetic field is turbulent and it is assumed to be advected with the jet as in Blandford and Koenigl (1979). The jet begins near equipartition as noted in Table 2. From equation 1, the value of $m_{\text{base}} = 2.64$ means that magnetic energy is dissipated rapidly in the plasma near the base of the jet. The lost energy is the X-ray emission forming the high energy power law. The core is the most powerful portion of the jet and most of the energy is lost to X-rays by inverse Compton cooling. The X-ray spectrum is computed per the methods of Tucker (1975); Ghisellini et al (1996); Sambruna et al (1997). The X-ray power law spectral index, $(p-1)/2$, fixes $p = 5.6$. This is a very steep value that is consistent with the assumption of intense Compton cooling. The disk emission is fit by a simple blackbody (instead of a parameterized accretion disk model) with $T = 1.5 \times 10^7$ ° K and a surface area on each disk face of 2.4×10^{14} cm² (the surface area of a thin Keplerian disk for $r \leq 5M$ and $a/M = 0.99$). The

spectral fit has $\approx 4.0 \times 10^{38}$ ergs/sec in thermal disk luminosity and $\approx 2.5 \times 10^{38}$ ergs/sec in jet luminosity (note the total matches that inferred by Fuchs et al (2004) when the flux overestimate from RXTE/PCA of 16% that they note is taken into account). The large EUV peak in the synchrotron spectrum in Figure 2 is from the same electrons that produce the EIC. The outer portion of the core jet at large z is inertially dominated and is a weak synchrotron source.

Shells 1 to 4 are Poynting flux dominated jets with a field line angular velocity, Ω_F , equal to the relativistic Keplerian velocity, Ω_{Kep} , at the foot point Lightman et al (1975). The field is organized and satisfies the perfect MHD condition similar to the electrodynamic models of Blandford (1976); Lovelace (1976),

$$B^\phi = \frac{\rho B^P (d\phi/dt - \Omega_F)}{v^P} . \quad (2)$$

The jets have an artificial simplification that the poloidal bulk velocity is constant, $v^P = 0.4c$. From equations (1) and (2), at large z , the toroidal magnetic field, B^ϕ , is much larger than the poloidal magnetic field, B^P , and the particle angular velocity, $d\phi/dt$, is small compared to Ω_F (bounded velocity and angular momentum). Perfect MHD requires that the total poloidal magnetic flux is conserved in each shell,

$$\Phi = \int B^P dA_\perp , \quad (3)$$

where dA_\perp is the cross-sectional area in the shell. Equations (1) - (3) combine to give a relationship between B^P at the base of the jet and B^ϕ at the start of the outer jet,

$$B_{\text{base}}^P \approx \left(\frac{v^P B_{\text{outer}}^\phi}{\rho_{\text{base}} \Omega_{\text{Kep}}} \right) \left(\frac{z_0(\text{outer})}{z_0(\text{base})} \right)^{0.5} . \quad (4)$$

This relationship allows one to compute (as in Table 2) Φ and the poloidal Poynting flux, S^P , in both regions of the jet, where

$$S^P = -\frac{1}{4\pi} \int \Omega_F \rho B^\phi B^P dA_\perp . \quad (5)$$

The base of the shell 1 jet produces the bulk of the synchrotron IR emission. The jet emission in K_s band was estimated to be about 40% of the total luminosity (the bulk being from the donor star) in Fuchs et al (2003) consistent with the fit in Figure 2. The value of $p = 3.3$ for the shells is chosen to reproduce the noticeable hardening of the X-ray spectrum above 10^{19} Hz seen in the INTEGRAL data in Figure 2 and discussed above. More than one half of this excess over the steep core powerlaw arises from EIC at the base of the shell 1 jet. The other shells provide the remainder of the hard EIC excess and the inner part of the brightness profile of the jet in Figure 3. Shell 4 is very energetic because the volume is huge - it has a very wide base. Shells 2 and 3 are required to interpolate the brightness distribution in Figure 3 between the "radio core" and base of the observed radio jet produced by the plasma in shell 4 and the distant regions of the brightness distribution that is emitted from plasma in shell 1.

In summary, if one assumes that the hard X-ray power law is produced in the jet (as in the fiducial model described in the last two sections) then the results in Table 2 imply that the jet power is $Q = 4.2 \times 10^{38}$ ergs/sec. Assuming $a/M = 0.99$, the mass flux in the jet is 7.8×10^{17} g/s.

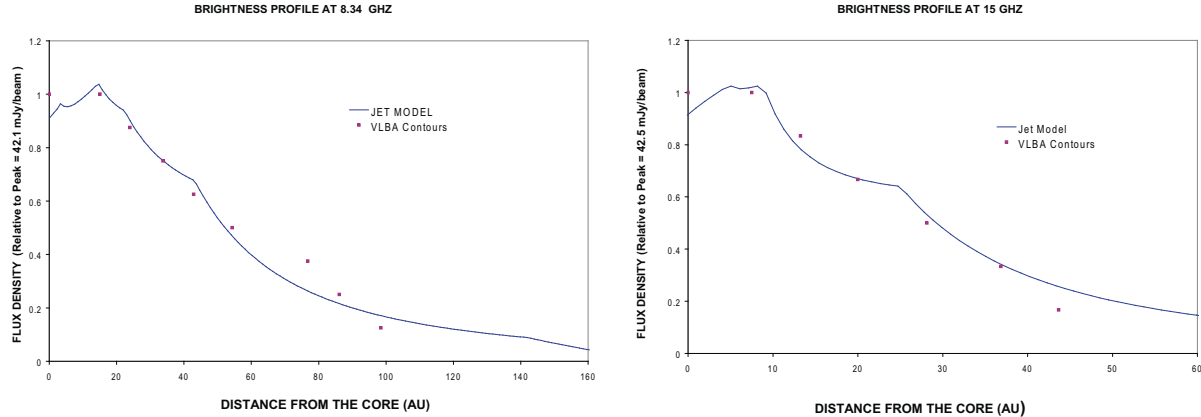


Figure 3. The brightness profiles at 8.3 GHz and 15 GHz obtained from the contours of the VLBA images in Fuchs et al (2004). Each dot represents a contour level. For comparison, the synthesized flux per beam that is produced from the 5 shell jet model convolved with the VLBA beamwidth and interstellar scattering is plotted. The diffuse nature of the jet emissivity requires a very broad base and transverse gradients in the jet, greatly increasing the volume and the required power. The excess flux at large z provided by the model is a desired effect, since simultaneous VLA measurements at 8.3 GHz in Fuchs et al (2003) show that $> 20\%$ of the flux is resolved out by VLBA and likely resides at large distances, $> 10^{15}$ cm. The plots do not cover the counter-jet as it was noted in Ribo et al (2004) and in the text that a single velocity cannot produce the asymmetry in the velocity profile, so there cannot be a good fit to this data simultaneously. This might be evidence that transverse and axial gradients in the bulk velocity are required or the jet model is not representative of the emission.

Table 1. Input Parameters of the Jet Component Models

Shell	m_{base}	n_{base}	a_{base}	m_{outer}	n_{outer}	a_{outer}	ϵ	$z_0(\text{outer})$ cm	$z_0(\text{base})$ cm	ρ_{base} cm
	a	b	a	a	b	a	a	a	a	c
0	2.64	2	1.52×10^3	2.4	2	3.82×10^3	0.45	1.0×10^8	5.0×10^6	3.4×10^6
1	1.08	2	4.02×10^3	2.1	2	2.20×10^2	0.595	1.5×10^{13}	5.0×10^6	8.8×10^6
2	1.02	2	6.03×10^3	1	2	1	0.8	4.0×10^{12}	5.0×10^6	1.4×10^7
3	0.99	2	1.35×10^4	1	2	5.0×10^{-2}	0.92	8.5×10^{12}	5.0×10^6	3.0×10^7
4	1.00	2	3.57×10^4	1	2	1.4×10^{-2}	1	6.5×10^{12}	5.0×10^6	8.0×10^7

Table 2. Table notes: a. input parameter for model fitted to SED data, b. set by baryon conservation, c. input parameter is a minimum value consistent with the black hole dimensions

4 PARAMETRIC SENSITIVITY

It is not claimed that this fiducial model is the unique jet solution that fits the data. This raises the question of how the model depends on the parametric assumptions. Although a formal parametric sensitivity analysis is beyond the scope of this work, many trial models were produced and evaluated in the process of arriving at the model presented in the previous sections. Here are some of the observations that were made.

- **Number of Shells** The integrated kinematic quantities such as the magnetic, energy and mass fluxes are not significantly affected by the number of shells. The more shells, the smoother the brightness distribution and the better the fit is in Figure 3. For example, if 4 or 6 shells were used instead of 5, the SED can be reproduced. However, the fit in Figure 3, would be considerably worse for 4 shells and somewhat better for 6 shells. The luminosity in each shell decays on scales that are comparable to the distance, z , that the peak of the luminosity is from the accretion disk. For example, the 15 GHz luminosity is produced at smaller z than the 8.3 GHz luminosity in each shell. Thus, the surface bright-

ness dies off with a shorter scale length at 15 GHz than at 8.3 GHz. Compare the right hand frame of Figure 3, to the left hand frame - the 15 GHz fit is worse in the sense that there are large curved sections between actual data points and a pronounced inflection point neither of which exist within the sparsely sampled data (there are only 6 contour levels in 15 GHz image in Fuchs et al (2004)). This is manifested as the almost exponential decay near 10 AU, followed by a sharp peak at ≈ 25 AU. The more shells, the less pronounced the alternating regions of exponential dips and sharp peaks become. With 4 shells, the 8.3 GHz plot would have similar large deviations from the brightness profile as are seen in the existing 15 GHz plot in Figure 3.

- **Energy Flux Estimate** Given the assumptions in the model (in order of importance: the hard X-ray luminosity is from the jet, the hard X-ray excess above 10^{19} GHz is real and from the jet, and the IR excess above the stellar contribution is from the jet), the model is very close to a minimum energy flux. This is obvious since the energy flux is only 1.5 times the radiated luminosity and the jet power must exceed the broadband luminosity. The energy flux grows very rapidly, if the jet is assumed to originate at large cylindrical

Table 3. Physical Parameters of the Jet Component Models

Shell	Q 10^{38} ergs/sec b	N cm^{-3} a	B Field a	B^ϕ 10^6 G b	B^P 10^6 G b	S/KE Base b	S/KE Outer b	Φ G - cm^2 b	p a	γ_{\min} a	γ_{\max} a
0	3.37	9.5×10^{17}	Turbulent	29.8	29.8	2.3	1.7×10^{-2}	Net = 0	5.6	1.5	1000
1	0.12	2.9×10^{11}	MHD Jet	6.9	3.3	4.8×10^4	2.1×10^4	1.4×10^{21}	3.3	50	1000
2	0.04	1.3×10^{10}	MHD Jet	2.6	2.3	3.4×10^5	2.6×10^5	8.4×10^{20}	3.3	50	1000
3	0.18	2.7×10^9	MHD Jet	2.1	3.0	1.1×10^6	1.1×10^6	4.7×10^{21}	3.3	50	1000
4	0.49	8.4×10^8	MHD Jet	1.1	2.9	1.0×10^6	1.0×10^6	2.0×10^{22}	3.3	50	1000

Table 4. Table notes: a. input parameter for model fitted to SED data, b. derived quantity from parameters of the jet model

radius. The volume of plasma and fields increases rapidly and the energy flux quickly rises above 10^{39} ergs/sec as the cylindrical radii of the base of the shells increase by a factor of $\gtrsim 2$.

- **Number Density** The number of energetic particles is fixed by the location of the base of the jet, the thermal X-ray flux from the accretion disk and the constraints on the observed external Compton luminosity. The particle flux and energy flux are concentrated at small radius in the core. Driving most of the energy and mass flux from the inner region of the disk is favored on physical grounds. It co-locates the most energetic shell and largest mass flux at the largest potential source of power to drive the jet - the most energetic part of the accretion flow (fastest rotation rate and highest temperature). Moving the core to the smallest possible cylindrical radius also moves the other shells inward to smaller radius and larger Keplerian velocity, thereby decreasing the total volume and magnetic flux required to drive the flow, by equation (5). This minimizes the energy flux in the outer shells. In this decomposition, the mass flux in the outer shells is constrained by the magnitude of the hard X-ray excess above 10^{19} Hz (EIC from shells 1 -4) discussed in section 2. The large radio fluxes from the outer shells combined with a modest EIC X-ray component result in the magnetic dominance for the outer shells depicted in columns 7 and 8 of Table 2. This analysis does not preclude the possibility of a different transverse distribution of mass flux in a jet that can reproduce the data, however the energy flux is likely to be larger.

- **Magnetic Field Strength** The magnetic field strength, B is set by the size of the base of the jet, the particle number density and the synchrotron portion of the SED. The magnetic field must also be of sufficient strength to be the ultimate energy reservoir that supports the bulk of radiation losses as discussed in section 3.

- **Electron Energy Spectrum** The electron spectrum is fixed by the X-ray power law spectrum as mentioned in section 2. The only parameter that is not affected by the data is Γ_{max} . Since the energy distributions are steep, there are very few high energy electrons. A value of $\Gamma_{max} = 1000$ was chosen arbitrarily. Any value larger than 700 will show negligible differences in the results.

- **Axial Dimensions** The value of $z_0(\text{base})$ is set by the physical dimensions of the accretion/disk black hole system. The quantities defined at $z_0(\text{base})$ form the initial data for the initial surface of the entire jet. By contrast, $z_0(\text{outer})$ is set by the SED fit. For example, large values of $z_0(\text{outer})$ over-produce the high frequency synchrotron emission. By

definition $z_0(\text{outer}) \equiv z_{\max}(\text{base})$. The solution is insensitive to $z_{\max}(\text{outer}) = 5 \times 10^{15}$ cm, since the jet emissivity is very low in this region.

5 ALTERNATIVE MODELS

The shell decomposition in Table 2 is very useful for exploring variants of the jet model. The most obvious variant is to assume that the disk corona and not the jet is the source of the X-ray powerlaw. By lowering the mass density and magnetic field density significantly (say, a factor of 100 for the sake of argument) in the core, one can simply ignore the energy flux and luminosity contribution to the composite jet. Then summing the remaining components in Table 2,

$$Q \approx 8.3 \times 10^{37} \text{ ergs/sec}, \text{ for a coronal X-ray source,} \quad (6)$$

and the jet plasma still reproduces the SED (less the coronal X-rays) and the radio brightness profile in Figures 2 and 3, respectively.

There is uncertainty in the non-relativistic jet velocity as noted in Section 1. Thus, it is desirable to know the sensitivity of the jet power to different values of jet poloidal velocity, $Q(v^P)$. The shell model lends itself to estimating Q for different values of v^P . First decompose Q into 3 discrete pieces. Then note from equations (2) and (5), that S^P in the outer jet has a simple scaling with v^P , $S_{\text{outer}} \sim v^P (B^\phi)^2$. Since Q is a sum of radiation losses, the mechanical kinetic energy flux in the outer jet, KE , and S_{outer} , one can use the results in Table 2 to parameterize Q as a function of v^P when the X-ray power law is from the jet. Implementing the Doppler enhancement factors from Lightman et al (1975),

$$\begin{aligned}
 Q(v^P) \approx & \left[\frac{\delta(\beta = 0.4, \theta = 70^\circ)^4 + \delta(\beta = -0.4, \theta = 70^\circ)^4}{\delta(\beta, \theta = 70^\circ)^4 + \delta(-\beta, \theta = 70^\circ)^4} \right] \\
 & \times (2.5 \times 10^{38}) \\
 & + \left[\frac{\delta(\beta = -0.4, \theta = 0^\circ)^4}{\delta(-\beta, \theta = 0^\circ)^4} \right]^4 (\Gamma - 1)(v^P/0.436c)(8.5 \times 10^{37}) \\
 & + (v^P/0.4c)(8.3 \times 10^{37}) \text{ ergs/sec,} \quad (7)
 \end{aligned}$$

where $\delta \equiv \delta(\beta, \theta)$, the Doppler factor that was introduced in Section 1, is a two parameter function of β and θ . In this notation, $\delta(\beta = 0.4, \theta = 70^\circ)$ means to evaluate the Doppler factor at $\beta = 0.4$ and $\theta = 70^\circ$. The jet poloidal velocity is $v^P \equiv c\beta$.

The Doppler correction on the first term in equation (7), means that larger δ factors require smaller intrinsic radiation losses to produce the observed X-ray powerlaw SED in

Figure 2. The Doppler correction on the second term results from the redshifting of the disk thermal emission in the rest frame of the plasma at the base of the jet. A slow jet sees a stronger seed field and requires fewer hot particles to reproduce the EIC SED and therefore has a smaller bulk kinetic energy flux. The last term is the electromagnetic energy flux in the outer jet. As noted in section 1, this formula will not hold for large β since SSC contributions become important.

Similarly, if the disk corona is the source of the X-ray powerlaw, one can use the results in Table 2 and equation (6) to parameterize the jet power as a function of jet velocity as

$$Q(v^P) \approx [v^P/0.4c][8.3 \times 10^{37}] \text{ ergs/sec} . \quad (8)$$

6 DISCUSSION

The crude model presented here has demonstrated a few facts about the compact jet in GRS 1915+105 in the "high plateau state":

- It is possible to model the jet in a manner analogous to AGN
- The jet is powered during a high accretion state with a thermal luminosity of $\approx 4 \times 10^{38}$ ergs/sec, corresponding to an Eddington rate of $\approx 23\%$.
- The jet brightness profile requires a highly stratified jet in the transverse direction
- Relativistic jet bulk velocity is not favored based on the huge implied energy flux, $> 3.5 \times 10^{40}$ ergs/sec if the jet is the source of the X-ray power law.

An interesting consequence of the model was that a rapidly spinning black hole was preferred on energetic grounds. This was not to tap black hole spin energy, but to use the surface area and high angular velocity of the plasma in the ergosphere to power the jet core. It is interesting to note that the 3-D, perfect MHD, general relativistic numerical simulations in Hawley and Krolik (2006) find very high efficiency "funnel wall jets" emanating from this region of the ergosphere of high spin black holes. The outflow is somewhat similar to what is described in the core shell in this treatment, near equipartition with turbulent disordered magnetic flux and an outflow velocity of $\sim 0.3c$. The efficiency is sufficient to power the core if $a/M > 0.95$. They argue that the power source is pressure gradients driven by the disk which seems energetically reasonable in GRS 1915+105 considering the large thermal luminosity noted above.

Even though there is some numerical evidence to support the notion of a near-relativistic jet core (where most of the energy transport occurs), it is not clear if there is any analog of the compact jet in the AGN population. In particular, are there near-relativistic outflows that are highly stratified in the transverse direction that carry a mass flux comparable to the accretion flux? It is also not obvious if there is any structure that can be construed as an analog of a non-relativistic high luminosity, optically thick, radio jet in AGN. If there is scale invariance in black hole accretion systems then there should be an analog of the compact jet in some AGN. The only obvious way to reconcile this difference is to consider the possibility that an AGN radio jet analogy is not appropriate and the analog of the compact jet in AGN takes a different guise due to the lower accretion disk

temperature. The AGN feature that possesses the majority of the characteristics of the jet model of GRS 1915+105 are the near-relativistic outflows that are seen in X-ray absorption. A few radio quiet quasars have been observed to have out-flowing, X-ray absorbing winds with velocities between $0.1c$ and $0.6c$ (Chartas et al 2003; Gofford et al 2011; Pounds et al 2003; Saez et al 2009). The outflow in APM08279+5255 is the most energetic with a mass flux similar to the accretion mass flux and a kinetic luminosity comparable to the thermal luminosity of the accretion flow as in GRS 1915+105 (Saez et al 2009). The fastest known out-flowing, X-ray absorbing winds in radio loud AGN have $v < 0.15c$ (Tombesi et al 2010).

In summary, due to the relatively low jet velocity and the large transverse stratification, perhaps the compact jet in black hole binaries is best described as a bipolar near-relativistic wind. In this analogy, it is not obvious why the Galactic black hole version of the wind is luminous in the radio band and the AGN version is not.

It has been argued in Koerding et al (2006) that there may exist a compact, optically thick jet in low-luminosity AGN. This may or may not be applicable to the study here in that the thermal luminosity was 23% of the Eddington limit in these observations of GRS 1915+105. In any event, it is worthwhile to study jets from low luminosity AGN with VLBI to look for evidence of nonrelativistic optically thick winds or jets.

The implication of these jet models to other Galactic black holes can only be speculated upon because other sources do not have the wealth of high resolution radio images. Furthermore, GRS 1915+105 is a very strong X-ray source, so there are many excellent studies of the radio jet/ X-ray connection. Consider, the results of Rushton et al (2010b); Rodriguez et al (2008) that the existence of a hard power-law component is tantamount to the existence of a jet. Within the framework of the assumption that inverse Compton emission in the jet is the dominant source of the power law component, the jet power can be estimated from the model presented here as approximately 1.5 times the hard X-ray power law luminosity. This estimate can be applied to other Galactic black holes in the hard state. However, it would be much more accurate to constrain the energy flux derived from the basic jet model on a case by case basis with deep radio images and broadband simultaneous spectroscopy, which are not readily available for other Galactic black holes. There are estimates of the compact jet energy flux based on less direct methods for other black hole candidates such as Cygnus X-1. For example, the emission from a nebular ring 5 pc from Cygnus X-1 has been used to estimate the energy flux required to energize the structure. This in turn is related to the compact jet power on much smaller scales by assuming an invisible flow of energy to large scales. This leads to estimates of the kinetic power of the compact jet of 10^{36} to 10^{37} ergs/sec (Gallo et al 2005; Russell et al 2007). This estimate is 0.3 to 1.0 of the total radiative luminosity, which is similar to the jet power of approximately 0.6 times of the total radiative luminosity that was found for the compact jet in GRS 1915+105 here.

Another consequence of the model is that a relativistic outflow velocity in compact jets is not favored based on energetic concerns. It is interesting to compare this to less direct estimates of the compact jet speed in GRS 1915+105 and

other Galactic black hole candidates. Using the very basic jet model of Blandford and Koenigl (1979), it is argued in Casella et al (2010) that $\Gamma > 2$ in GX 339-4, which was have ruled out for GRS 1915+105 in the epoch considered here. A very general argument was presented in Heinz and Merloni (2004) that was based on total X-ray and radio fluxes from a one zone model (that happens to be cylindrical in shape). They found a loose set of constraints that favored $\Gamma > 2$ in Galactic X-ray binaries, but was also consistent with $\beta \approx 0.5$. Contrary to these works Gallo et al (2003) used Monte Carlo simulations to argue that $\Gamma \lesssim 2$ is preferred for Galactic X-ray binaries in the low/hard state, marginally consistent with the energetic constraints of the models presented here.

ACKNOWLEDGMENTS

I am indebted to Jerome Rodriguez for analyzing the X-ray data and discussing the implications with me. I would also like to thank Marc Ribo for useful discussions regarding the radio data. I was lucky to have a referee who offered many suggestions that improved the presentation of the manuscript.

REFERENCES

- Blandford, R. D. 1976, MNRAS **176** 465
 Blandford, R. and Konigl, A. 1979, ApJ **232** 34
 Casella, P. et al, 2010, MNRAS Lett. **404** 21
 Chartas, G., Brandt, W.N., Gallagher, S. 2003, ApJ **595** 85
 Dwahan, V., Mirabel, I.F., Rodriguez, L. 2000, ApJ **543** 373
 Fender, R. et al, 1999, MNRAS **304** 865
 Fuchs, Y. et al, 2003, A and A **409** L35
 Fuchs, Y. et al, 2004, Proc. of the 5th INTEGRAL Workshop (ESA) <http://xxx.lanl.gov/abs/astro-ph/0404030>
 Gallo, E., Fender, R., Pooley, G. 2003, MNRAS **344** 60
 Gallo, E. et al 2005, Nature **436** 819
 Ghisellini, G., Maraschi, L. and Treves, A., 1985, A & A **146** 204
 Ghisellini, G. and Maraschi, L., 1989, ApJ **340** 181
 Ghisellini, G., Maraschi, L. and Dondi, L., 1996, Suppl. Series A & A **120** 503
 Gofford, J., et al 2011, MNRAS **414** 3307
 Greiner, J., Cuby, J., McCaughrean, M. 2001, Nature **414** 522
 Hawley, J., Krolik, K. 2006, ApJ **641** 103
 Heinz, S., Merloni, A. 2004, MNRAS Lett. **355** L1
 Koerding, E., Jester, S., Fender, R. 2006, MNRAS **372** 1366
 Lightman, A., Press, W., Price, R. and Teukolsky, S. 1975, *Problem Book in Relativity and Gravitation* (Princeton University Press, Princeton)
 Lind, K., Blandford, R. 1985, ApJ **295** 358
 Lovelace, R. V. E. 1976, Nature **262** 649
 Markoff, S., Nowak, M., Wilms, J. 2005 ApJ **635** 1023
 Mirabel, I.F., Rodriguez, L. 1994, Nature **371** 46
 Murray, N., Chiang, J., Grossman, S., Voit, G. 1995 ApJ **451** 198
 Ogley, R., Bell Burnell, S. Fender, R., Pooley, G., Waltman, E. 2000, MNRAS **317** 158
 Pooley, G. and Fender, R. 1997, MNRAS **292** 925
 Pounds, K., King, A., Page, K., O'Brien, P. 2003, MNRAS **346** 1025
 Reeves, J., et al 2009, ApJ **701** 493
 Ribo, M., Dhawan, V. Mirabel, F. 2004, Proc. of the 7th VLBI Network Symposium, Bachiller, R., Colomer, F., Desmurs, J., de Vicenete, P. (eds) Toledo, Spain astro-ph/0412657
 Rodriguez, J., et al 2004, ApJ **615** 416
 Rodriguez, J., et al 2008, ApJ **675** 1436
 Rodriguez, L., Mirabel, I.F. 1999, ApJ **511** 398
 Rushton, A., Spencer, E., Fender, R. and Pooley, G. 2010, A & A **524** 29
 Rushton, A., Spencer, E., Pooley, G., Trushkin, S. 2010, MNRAS **401** 2611
 Russell, D., Fender, R., Gallo, E., Kaiser, C. 2007, MNRAS **376** 1341
 Saez, Chartas, G., Brandt, W.N. 2009, ApJ **697** 194
 Sambruna, R. et al 1997, ApJ **474** 639
 Tombesi, F., et al 2010, ApJ **719** 700
 Tucker, W. 1975, *Radiation Processes in Astrophysics* (MIT Press, Cambridge).